SPATIAL CORRELATION IN INDOOR MIMO CHANNELS

D.P. McNamara, M.A.Beach and P.N. Fletcher

Centre for Communications Research, University of Bristol,
Queen's Building, University Walk, Clifton, Bristol. BS8 1TR. UK.
Darren.McNamara@bristol.ac.uk

Abstract - This paper presents the analysis of spatial correlation in MIMO channels, calculated from data measured in office environments at 5.2GHz. Results are compared with those from channels generated using a stochastic MIMO channel model and the effect of different comparison metrics is shown. The suitability of the stochastic model under different propagation conditions is also investigated.

Keywords - MIMO propagation, channel measurement, channel model, spatial correlation.

I. Introduction

Numerous MIMO channel measurement campaigns, both narrowband and wideband, have been reported in the literature, several of which have been used as the basis for the development and parameterisation of stochastic MIMO channel models [1–3]. Of the parameters considered by these models, the most difficult to quantify is that of spatial correlation between elements at the two arrays. This is determined by both the propagation environment and the array configuration, through the power-angle distribution of multipath signals impinging on each array and the element types and spacing. Although the array architecture can be controlled, spatial correlation amongst the elements of the array is a function of the particular environment in which the arrays are located and has been the subject of much research in single array systems [4].

This paper presents the results of an investigation into the spatial correlation experienced by the two arrays in a narrowband MIMO system, based on wideband measurements recorded in a modern building at 5.2GHz. Measurement data is used to derive the spatial correlation parameters for a stochastic channel model, the output of which is compared with the measured channel responses. The effect of different parameter extraction techniques and their suitability under different propagation conditions is illustrated. The analysis initially examines non-line-of-sight (NLOS) channels, followed by some results under line-of-sight (LOS) conditions.

II. Channel measurements

Wideband MIMO channel measurements have been conducted using a Medav RUSK BRI channel sounder, as described in [5]. The arrays employed during these measurements were eight-element, vertically polarised, uniform linear arrays at both the transmitter and receiver (see [5] for photographs). The transmit array comprised of monopole elements, half-wavelength spaced and mounted on a horizontal rectangular groundplane, whilst the receive array was a commercially built unit consisting of cavity backed dipole elements, half-wavelength spaced and mounted so as to provide a 120degree half-power beamwidth.

The measurement campaign was conducted in a modern building, although the layout was a traditional office corridor with individual offices to either side, as shown by the floor plan in Figure 1. The receive array was located at one end of the corridor, at a height of 1.9m, and the transmitter was placed on a low trolley with the array mounted at a height of 0.9m. For each office in turn, the transmitter was slowly pulled across the centre of the room (a distance of approximately 2m) whilst the receiver recorded 2000 realisations of the 8×8 MIMO channel. This procedure was repeated with the transmit array having been rotated by 90degrees in azimuth. Finally, for those offices in which space permitted, a third set of 2000 channel realisations was recorded with the transmit array being moved and rotated in random directions.

Each realisation of a narrowband MIMO channel consists of the absolute transmission coefficients between all transmit and receive elements, and is represented (at frequency f) by the matrix $\mathbf{G}_f \in \mathbb{C}^{n_R \times n_T}$, whose elements are denoted as $g_{jk,f}$, for $j \in [1, 2, \ldots, n_R]$ and $k \in [1, 2, \ldots, n_T]$, where n_R and n_T are the number of receive and transmit elements respectively. A normalised channel matrix, $\mathbf{H}_f$, can hence be obtained as

$$\mathbf{H}_f = \frac{\mathbf{G}_f}{\sqrt{\frac{1}{n_R n_T F} \sum_{j=1}^{n_R} \sum_{k=1}^{n_T} \sum_{l=1}^{F} |g_{jk,l}|^2}}, \qquad (1)$$

where F is the number of discrete frequencies contained in each wideband measurement. Note that during the following analysis, even when subsets of the array elements are selected, each channel realisation is first normalised as in (1) with $n_R, n_T = 8$ and $F = 97$, so as to obtain the best estimate of the local mean path loss.

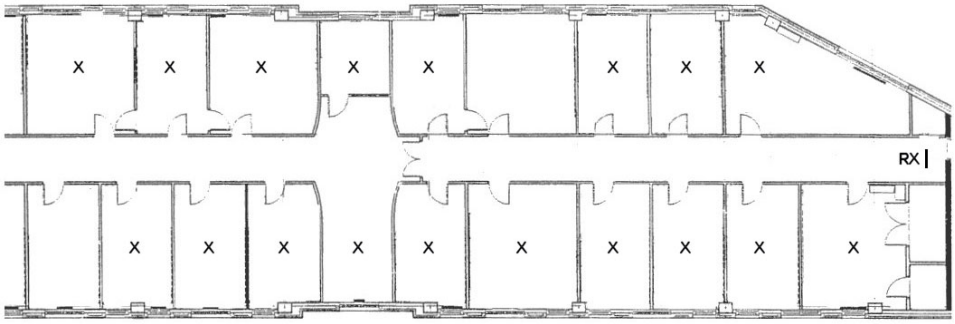

Fig. 1. Measurement environment. X denotes locations of the transmitter from which measurements were recorded.

III. Stochastic MIMO channel model

The basic structure of the model presented here is common to several published stochastic MIMO models [1–3]. In this paper we only consider the narrowband case as described below.

A narrowband MIMO channel in a quasi-static, Rayleigh fading environment with no spatial correlation, $\mathbf{A} \in \mathbb{C}^{n_R \times n_T}$, can be generated by taking all elements to be i.i.d. zero-mean unit-variance complex Gaussian random variables.

In [1–3] it is proposed that the introduction of spatial correlation is made easier if it can be assumed that correlations amongst the elements of one array are independent of the selected antenna element at the other array. This assumption is justified by the reasoning that each element within an array will illuminate the same scatterers in the surrounding environment. The energy arriving at the second array from each of the transmit elements will therefore exhibit the same power-angle spectrum and hence the same spatial correlation [1].

If the complex correlation coefficient between two elements at the receiver, j_1 and j_2, is represented by

$$\rho^{\mathrm{RX}}_{j_1 j_2} = \langle g_{j_1 k},\, g_{j_2 k} \rangle\,, \tag{2}$$

then the above assumption dictates that this value is independent of k. A matrix of these correlation coefficients $\mathbf{R}_{\mathrm{RX}} \in \mathbb{C}^{n_R \times n_R}$ can then be constructed such that

$$\mathbf{R}_{\mathrm{RX}} = \begin{bmatrix} \rho^{\mathrm{RX}}_{11} & \rho^{\mathrm{RX}}_{12} & \cdots & \rho^{\mathrm{RX}}_{1n_R} \\ \rho^{\mathrm{RX}}_{21} & \rho^{\mathrm{RX}}_{22} & \cdots & \rho^{\mathrm{RX}}_{2n_R} \\ \vdots & \vdots & \ddots & \vdots \\ \rho^{\mathrm{RX}}_{n_R 1} & \rho^{\mathrm{RX}}_{n_R 2} & \cdots & \rho^{\mathrm{RX}}_{n_R n_R} \end{bmatrix}. \tag{3}$$

Given a similar definition of $\rho^{\mathrm{TX}}_{k_1 k_2}$ and $\mathbf{R}_{\mathrm{TX}} \in \mathbb{C}^{n_T \times n_T}$, and following suitable selection of all ρ^{TX} and ρ^{RX}, a correlated channel matrix can be generated as [6]

$$\mathbf{H}_{\mathrm{sim}} = (\mathbf{R}_{\mathrm{RX}})^{1/2}\, \mathbf{A}\, ((\mathbf{R}_{\mathrm{TX}})^{1/2})^{\dagger}, \tag{4}$$

where $(\cdot)^{1/2}$ and $(\cdot)^{\dagger}$ denote the matrix square root and conjugate transpose respectively.

Therefore, in order to use this model, the array correlation matrices, $\mathbf{R}_{\mathrm{TX}}$ and $\mathbf{R}_{\mathrm{RX}}$, have to be defined, either arbitrarily or empirically. Given the aforementioned assumption that the spatial correlation at each array is independent of the element selected at the other array, it can be shown that the channel correlation matrix, $\mathbf{R}_{\mathrm{H}} \in \mathbb{C}^{n_R n_T \times n_R n_T}$, can be given by the Kronecker product of the array correlation matrices [7],

$$\mathbf{R}_{\mathrm{H}} = \mathbf{R}_{\mathrm{TX}} \otimes \mathbf{R}_{\mathrm{RX}}, \tag{5}$$

where $\otimes$ denotes the Kronecker product.

$\mathbf{R}_{\mathrm{H}}$ can be estimated from channel measurement data as

$$(\mathbf{R}_{\mathrm{H}})_{pq} = \left\langle \mathrm{vec}(\mathbf{H}_f)_p,\, \mathrm{vec}(\mathbf{H}_f)^{\dagger}_q \right\rangle,\ p, q \in [1, 2, ..., n_R n_T], \tag{6}$$

where $\mathrm{vec}(\cdot)$ is the vector operator and p and q denote the element index within a matrix or vector appropriately. Therefore, employing the method described in [8], $\mathbf{R}_{\mathrm{TX}}$ and $\mathbf{R}_{\mathrm{RX}}$ can be calculated using the rank one least squares Kronecker factorisation of $\mathbf{R}_{\mathrm{H}}$. This computes the factors $\mathbf{R}_{\mathrm{TX}}$ and $\mathbf{R}_{\mathrm{RX}}$ to satisfy

$$\min || \mathbf{R}_{\mathrm{H}} - \mathbf{R}_{\mathrm{TX}} \otimes \mathbf{R}_{\mathrm{RX}} ||_F, \tag{7}$$

where $|| \cdot ||_F$ denotes the Frobenius norm. A metric for the error resulting from this approximation can be found by calculating

$$\Psi(\mathbf{X}, \mathbf{Y}) = \frac{||\mathbf{X} - \mathbf{Y}||_F}{||\mathbf{X}||_F}, \tag{8}$$

where $\mathbf{X}$ and $\mathbf{Y}$ are $\mathbf{R}_{\mathrm{H}}$ and $(\mathbf{R}_{\mathrm{TX}} \otimes \mathbf{R}_{\mathrm{RX}})$ respectively [8].

The effect of the approximation resulting from (7) can also be investigated by comparison between the channels generated in (4) with those generated according to the full correlation properties given by $\mathbf{R}_{\mathrm{H}}$. The latter can be achieved by redefining (4) as

$$\mathrm{vec}(\mathbf{H}_{\mathrm{sim}}) = (\mathbf{R}_{\mathrm{H}})^{1/2} \mathrm{vec}(\mathbf{A}). \tag{9}$$

Herein, we refer to the two models, (4) and (9), as the 'Kronecker' model and the '$\mathbf{R}_{\mathrm{H}}$' model.

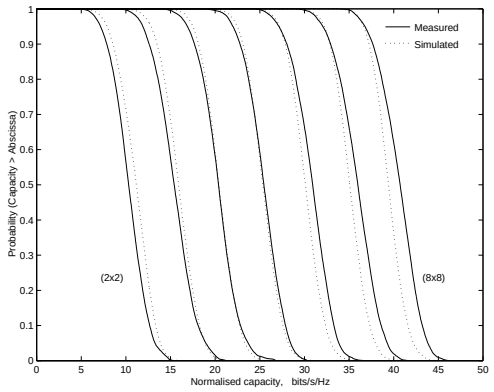

Fig. 2. Capacity CCDFs for the channels measured in one office and channels generated using the Kronecker model with parameters derived from the measured data. Results for array sizes from 2×2 to 8×8 are shown, with $n_R = n_T$.

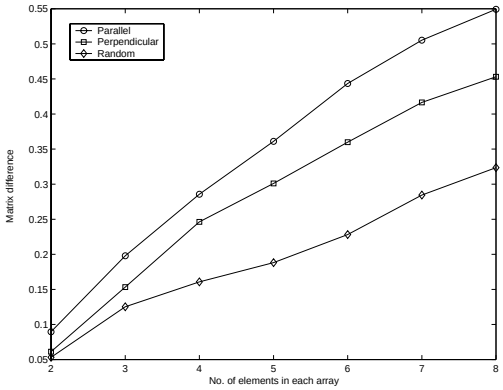

Fig. 3. Mean difference between the Kronecker product of the array correlation matrices and the channel correlation matrix, for varying array sizes and orientations of the TX array with respect to the office door.

IV. Data analysis

We initially investigate the accuracy of the Kronecker model by comparing it with measured data on an office by office basis, and for varying numbers of array elements, from 2×2 to 8×8, with $n_R = n_T$. For each office in turn, appropriately sized subsets of data are selected from the normalised measured channel matrices (transmit elements $1, ..., n_T$ and receive elements $1, ..., n_R$). From this data, the array correlation matrices, $\mathbf{R}_{\mathrm{TX}}$ and $\mathbf{R}_{\mathrm{RX}}$, are estimated as described in Section III and used to generate a set of stochastic channels. The capacities of both sets of channels are then calculated as

$$C = \log_2 \left(\det \left(I_{n_R} + \frac{\rho}{n_T} \mathbf{H}\mathbf{H}^{\dagger} \right) \right) \quad \text{bits/s/Hz}, \quad (10)$$

where I_n is the $n \times n$ identity matrix, $\det(\cdot)$ is the matrix determinant, and ρ is the mean signal to noise ratio at each receiver (in this paper ρ is kept constant at 20dB). From this, the capacity complementary cumulative distribution functions (CCDFs) can be generated, as shown by the example in Figure 2 for one of the offices.

Two metrics are used for the comparison between modelled and measured data. Firstly, the difference between the Kronecker product of the approximated array correlation matrices and the channel correlation matrix, Ψ, is calculated, as in (8), in order to quantify the error in the Kronecker factorisation. Secondly, the performance of the model (defined here as the closeness of the modelled channels to the measured data) is assessed by calculating, Φ, the root mean square (r.m.s.) difference between the capacity CCDFs of the measured and simulated channels, normalised to the mean capacity of the measured channels.

For each of the measurement locations (and TX array orientations) shown in Figure 1, the measured and simulated capacity CCDFs have been generated as described above and in each case, the two aforementioned metrics calculated. Figure 3 shows how the first metric, Ψ, averaged over all locations, varies with the number of array elements and the array orientation. The variation in Ψ can be regarded as an indication of the validity of the initial assumption made by the Kronecker model; that the spatial correlation at each array is independent of the element selected at the other array. This follows from the use of the rank one approximation of (a permuted) $\mathbf{R}_{\mathrm{H}}$, employed in computing the solution to (7) [8]. If the model's assumption was exactly true, then the permuted matrix would be rank one, and hence $\mathbf{R}_{\mathrm{TX}}$ and $\mathbf{R}_{\mathrm{RX}}$ could be found such that $\Psi = 0$. Conversely, if $\Psi \neq 0$, this implies that the permuted $\mathbf{R}_{\mathrm{H}}$ is not rank one and hence the spatial correlation at each array is to some extent dependent on the element selected at the other array. The results in Figure 3 therefore suggest that by collecting data with random array orientations, a better fit with the model can be achieved.

Although the metric Ψ gives an indication of the error in representing the channel correlation matrix, $\mathbf{R}_{\mathrm{H}}$, as the Kronecker product of two array correlation matrices, $\mathbf{R}_{\mathrm{TX}}$ and $\mathbf{R}_{\mathrm{RX}}$, this is not necessarily a measure of how well the model (employing the parameters $\mathbf{R}_{\mathrm{TX}}$ and $\mathbf{R}_{\mathrm{RX}}$) actually performs at simulating channels of a similar nature to those from which the parameters were taken. Consequently, the difference in the distributions of channel capacities for the measured and simulated channels has been calculated as the second metric.

The scatter plot in Figure 4 shows the joint distribution of Φ, expressed as a percentage, and Ψ. It can be seen that the two metrics appear to vary independently and hence, for the data analysed here, the variations in Ψ due to the approximation in the Kronecker factorisation do not necessarily indicate how well the resultant parameters, $\mathbf{R}_{\mathrm{TX}}$ and $\mathbf{R}_{\mathrm{RX}}$, model the channel.

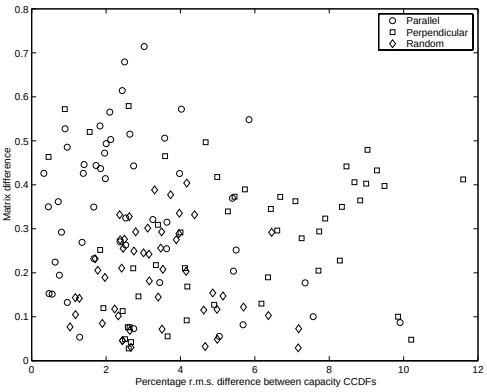

Fig. 4. Comparison between the two metrics employed for evaluating the channel models. Data is shown for the three orientations of the TX array with respect to the office door.

In order to further quantify the performance of the Kronecker model, we compare it with the $\mathbf{R}_{\mathrm{H}}$ model. Table 1 presents the mean and variance of Φ (calculated over all locations) for both models and for each of the TX array orientations. It also includes the results of the same analysis having been conducted using power rather than complex correlation for (2) and (6), as has also been suggested [1]. Comparing the values in the table, it can immediately be seen that both models employing complex correlation parameters perform well *for this data*, and much better than those based on power correlation.

Although the results in Table 1 look favourable for the Kronecker model, it should be noted that the data on which this investigation has been conducted so far has all been from relatively 'good' NLOS situations, since in order to provide a fair comparison between the TX array orientations, only those offices in which data for all three orientations was recorded have been considered so far. It just happens that the propagation characteristics in these locations were favourable for fitting to the Kronecker model. Other locations are no so suitable, as shown by the comparison between the two models in Figure 5. Here, it can be seen that although the $\mathbf{R}_{\mathrm{H}}$ model still performs well, with a close fit between the measured and simulated capacities, the Kronecker model is not suitable for array sizes larger than 2×2. The reason for this is that the spatial correlation at each array is no longer independent from the element selected at the other array, resulting in the key assumption of the Kronecker model no longer being valid. Conversely, the $\mathbf{R}_{\mathrm{H}}$ model, which includes the full channel correlation properties, can still generate stochastic channels with similar properties to those of the measured data.

A visual indication of the spatial correlation (for the full 8×8 channel) in this particular location is given in Figure 6. Here, the elements of $\mathbf{R}_{\mathrm{H}}$ have been rearranged in order to give a more intuitive representation

Table 1
Statistics for, Φ, the percentage r.m.s. difference between measured and simulated capacity CCDFs.

		Complex Corr.		Power Corr.	
Data	Model	Mean	Variance	Mean	Variance
Parallel	Kron.	2.76	4.36	16.0	31.5
Parallel	$\mathbf{R}_{\mathrm{H}}$	3.27	4.51	16.5	36.4
Perp.	Kron.	5.53	7.91	16.6	38.6
Perp.	$\mathbf{R}_{\mathrm{H}}$	2.91	2.77	17.7	40.9
Random	Kron.	3.43	2.27	11.1	33.9
Random	$\mathbf{R}_{\mathrm{H}}$	3.59	5.78	14.0	40.9

than plotting $\mathbf{R}_{\mathrm{H}}$ directly. Each 'square' of 8×8 values represents the magnitude of the complex correlation coefficient between one transmission coefficient, h_{jk}, and all others. These are arranged such that, for example, the 'top-left square' displays the correlation between h_{11} and all other transmission coefficients, and the 'top-right square' displays the correlation between h_{18} and all other transmission coefficients. Thus it can be seen that there is significant variation across the elements of each array.

In the particular case shown here, it is suggested that the reason for this characteristic is that the close proximity of objects in this environment and the relative size of the arrays with respect to the dimensions of the corridor and office, allows some array elements to be shadowed

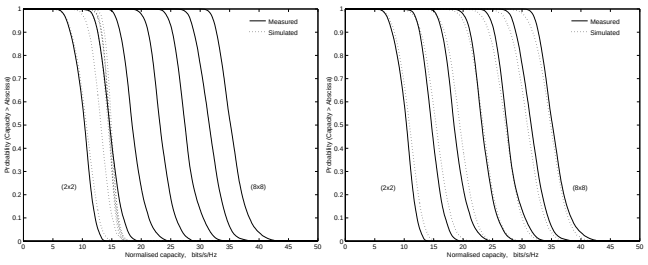

(a) Kronecker model (b) $\mathbf{R}_{\mathrm{H}}$ model

Fig. 5. Capacity CCDFs for the channels measured in one office and channels generated using, (a) the Kronecker model, and (b) the $\mathbf{R}_{\mathrm{H}}$ model, each with parameters derived from the measured data.

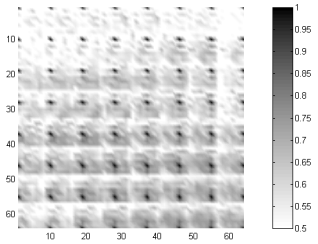

Fig. 6. Magnitudes of the complex correlation coefficients between all elements of the channel matrix, $\mathbf{H}$, for one office location.

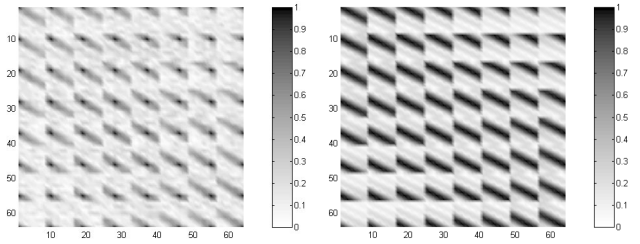

(a) Measured (b) Simulated

Fig. 7. Magnitudes of the complex correlation coefficients between all elements of the channel matrix, **H**, for data (a) measured in an empty room, and (b) simulated in free space.

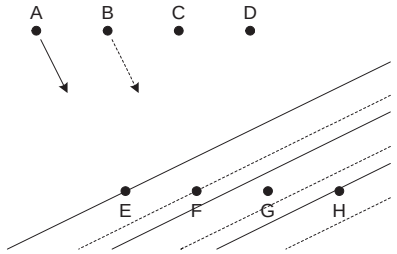

Fig. 8. Phase relationship between array elements for a MIMO system in free space.

when others are not. This does not necessarily have to be the case though, since similar analysis of other measured channel data has indicated that this effect is particularly prevalent under LOS conditions, or where a significant dominant path exists.

Although a full examination of the LOS case is beyond the scope of this paper, we introduce one particular characteristic of spatial correlation in LOS conditions.

Figure 7a shows the spatial correlation evaluated from data measured in a large empty room, where a direct, LOS, path always existed between the transmit and receive arrays [5]. It can be seen that the correlation exhibits a 'diagonal' pattern which should not be possible, since spatial correlation at either the transmit or receive array alone would result in 'horizontal' or 'vertical' regions of high correlation respectively.

This effect can be replicated by channels simulated in free space, as shown in Figure 7b. Here, given two uniform linear arrays sufficiently separated so that they are in each others far field (Figure 8), the transmission coefficients between A&E, B&F, C&G and D&H are equal, as are those between A&F, B&G and C&H etc. Therefore, when the *complex* correlation coefficients are calculated (6), the correlations between A and {E,F,G} are the same as those between B and {F,G,H}, leading to the diagonal appearance in Figure 7. Alternatively, if the *power* channel correlation coefficients were calculated, the relationship between the phase shifts across the arrays is irrelevant and all coefficients would equal 1.

The consequence of this is that the Kronecker model certainly cannot include this effect, since reality requires the correlation coefficients to vary with array element. In this case though, the $\mathbf{R}_{\mathrm{H}}$ model is also unsuitable since although it will generate channels with the specified complex correlation (as in Figure 7), the power correlation of the resultant channels will be incorrect. Therefore, for the example of the free space environment, the generated channel matrices are of much higher rank than the expected near rank one.

V. Conclusions

This paper has investigated the performance of two empirical stochastic MIMO channel models. The performance of the models has been shown to be good under NLOS propagation, although the Kronecker model was shown to fail under conditions where the correlation amongst the elements of one array was not independent of the antenna element at the other array. Finally, it was shown how situations in which array correlation does vary with array element can occur in LOS conditions, and how under these extreme circumstances, both stochastic models, as presented here, are unsuitable.

Acknowledgments

The authors gratefully acknowledge the financial contribution of the UK EPSRC, QinetiQ Ltd. and the IST SATURN project for their support of parts of this work.

References

[1] K.I. Pedersen, J.B. Anderson, J.P. Kermoal, and P. Mogensen, "A Stochastic Multiple-Input Multiple-Output Radio Channel Model for Evaluation of Space-Time Coding Algorithms," in *IEEE Conf. on Veh. Technol.*, Oct. 2000, Boston.

[2] K. Yu, M. Bengtsson, B. Ottersten, D.P. McNamara, P. Karlsson, and M.A. Beach, "A Wideband Statistical Model for NLOS Indoor MIMO Channels," in *IEEE Conf. on Veh. Technol.*, May 2002, Birmingham, AL.

[3] Lucent, Nokia, Siemens, and Ericsson, "A Standardized Set of MIMO Radio Propagation Channels," 3GPP TSG RAN WG1, R1(01)1179, Jeju, Korea, Nov. 2001.

[4] R.B. Ertel, P. Cardieri, K.W. Sowerby, T.S. Rappaport, and J.H. Reed, "Overview of Spatial Channel Models for Antenna Array Communication Systems," *IEEE Personal Communications*, vol. 5, no. 1, pp. 10–22, Feb. 1998.

[5] D.P. McNamara, M.A. Beach, P.N. Fletcher, and P. Karlsson, "Initial Investigation of Multiple-Input Multiple-Output Channels in Indoor Environments," in *IEEE Benelux Chapter Symp. on Commun. & Veh. Technol. (SCVT)*, Oct. 2000, Leuven, Belgium.

[6] D.-S. Shiu, G.J. Foschini, M.J. Gans, and J.M. Kahn, "Fading Correlation and Its Effect on the Capacity of Multielement Antenna Systems," *IEEE Trans. on Commun.*, vol. 48, no. 3, pp. 502–513, Mar. 2000.

[7] J.P. Kermoal, L. Schumacher, K.I. Pedersen, P.E. Mogensen, and F. Frederiksen, "A Stochastic MIMO Radio Channel Model with Experimental Validation," To appear in: IEEE J. Select Areas Commun., August 2002.

[8] K. Yu, M. Bengtsson, B. Ottersten, D.P. McNamara, P. Karlsson, and M.A. Beach, "Second Order Statistics of NLOS Indoor MIMO Channels based on 5.2 GHz Measurements," in *IEEE Globecom*, Nov. 2001, San Antonio.